ADVANCED HEALTHCARE MATERIALS
www.advhealthmat.de

Materials Views
www.MaterialsViews.com

Suppression of VEGF by Reversible-PEGylated Histidylated Polylysine in Cancer Therapy

Xiaojun Cai, Haiyan Zhu, Haiqing Dong, Yongyong Li, Jiansheng Su, and Donglu Shi**

A reversible-PEGylated polylysine is designed and developed for efficient delivery of siRNA. In this unique structure, the ε-amino groups of disulfide linked poly(ethylene glycol) (PEG) and polylysine (mPEG-SS-PLL) are partially replaced by histidine groups, in order to develop the histidylated reversible-PEGylated polylysine (mPEG-SS-PLH), for enhanced endosome escape ability. The transfection efficacy of mPEG-SS-PLH is found to closely correlate with histidine substitution. Its maximum transfection efficiencies are determined, respectively, to be 75%, 42%, and 24%, against 293T, MCF-7, and PC-3 cells. These data indicate that the transfection efficiencies can equal or even outweigh PEI-25k in the corresponding cells (80%, 38.5%, and 20%). The in vivo circulation and biodistribution of the polyplexes are monitored by fluorescent imaging. The in vivo gene transfection is carried out by intravenous injection of pEGFP to BALB/c mice using the xenograft models. The in vivo experimental results show effective inhibition of tumor growth by mPEG-SS-PLH/siRNA–VEGF, indicating its high potential for clinical applications.

1. Introduction

Clinical success of cancer interventions relies on the development of safe and efficient vehicles for gene transferring to target tissues.[1,2] Among various gene vectors, the nonviral vectors based on polycations have attracted great interests for their straight forward production routes, structural adaptability, large gene-carrying capacity, and safety.[3–5] A vast variety of polycations such as polyethylenimine,[6–9] dendrimers,[10–12] and polylysine[13–15] have been explored as gene vehicles with an appreciable success. However, gene therapy based on non-viral vector remains great challenges especially in delivering genes from a solution to the cell nucleus. The obstacles for gene delivery include extracellular (gene packaging, serum stability, cell-specific targeting) and intracellular barriers (endosome escape, efficient unpacking, transport through the cytoplasm and nuclear localization).[16–20] Hence, innovative approaches that address these critical issues of nonviral vectors are needed to offer viable therapeutic options in the future.

Polylysine is a conventional non-viral vector well known for its appreciable gene loading capacity. However, it's lacking of stability and capability of endosome escape has posted some limitations in the biomedical applications.[21–23] Recently, we have developed a reversible PEGylated polylysine that can efficiently pack gene and keep intact extracellularly while triggering the poly(ethylene glycol) (PEG) detachment according to the intracellular glutathione (GSH) level.[24–26] The key structural factor of this system relies on the disulfide link between the two blocks of PEG and polylysine. The redox-responsive property of the disulfide bond allows the selective detachment of PEG, facilitating the intracellular release and transfer of payload gene. The unique polylysine vector has been found to enhance the serum stability and gene transfection efficiency.

The present study aims at efficient delivery of siRNA–VEGF by reversible PEGylated polylysine for in vitro and in vivo cancer therapy. Small interfering RNA-vascular endothelial growth factor (siRNA-VEGF) has been widely used to suppress VEGF expression for inhibition of tumor growth and metastasis in cancer treatments.[27–29] The ε-amino groups of disulfide linked mPEG-SS-PLL are partially replaced by histidyl residues in order to construct the histidylated reversible-PEGylated polylysine (mPEG-SS-PLH) for enhancement of the endosome escape ability.[30–33] Lacking of amino groups, with a p*Ka* ≈ 5–7 for PLL, can lead to reduced "proton sponge effect" for endosomolysis and subsequent release of pDNA.[15,34,35] Previous reports have shown that incorporation of histidyl residues into PLL[33] or PEG–PLL[34] can increase transfection efficiency. However, without reversible-PEGylation, these carriers were

Dr. X. J. Cai, Dr. H. Q. Dong, Dr. Y. Y. Li, Prof. D. Shi
Shanghai East Hospital
The Institute for Biomedical Engineering and Nano Science
Tongji University School of Medicine
Tongji University
Shanghai 200120, China
E-mail: yongyong_li@tongji.edu.cn; donglu.shi@uc.edu
H. Y. Zhu, Prof. J. Su
Laboratory of Oral Biomedical Science and Translational Medicine Department of Prosthodontics
School of Stomatology
Tongji University
Shanghai 200072, China
Prof. D. Shi
Materials Science and Engineering Program
Department of Mechanical and Materials Engineering
College of Engineering and Applied Science
University of Cincinnati
Cincinnati, OH 10 45221, USA

DOI: 10.1002/adhm.201400063

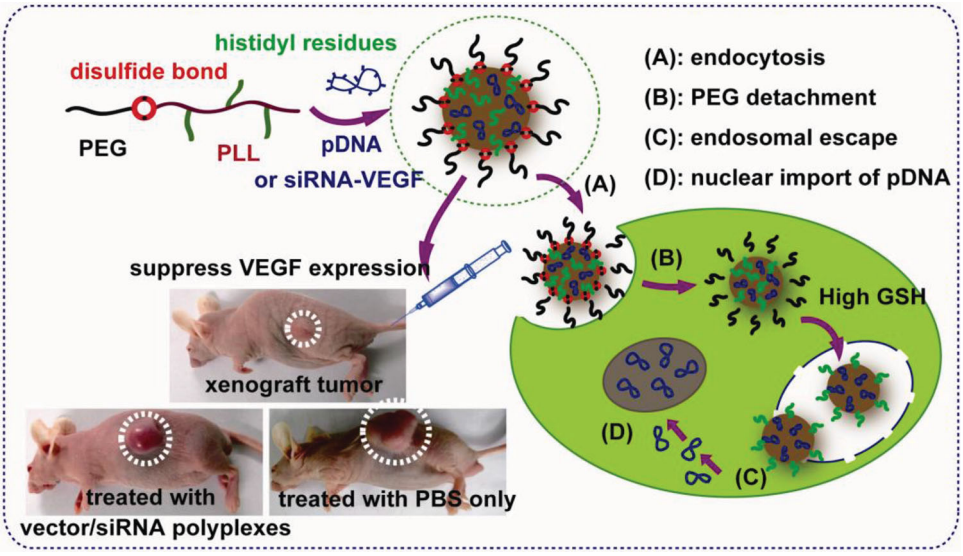

Scheme 1. Schematic illustration of reversible-PEGylated histidylated polyplex formation, subsequently intracellular dePEGylation, histidine-mediated endosomal escape, and in vivo cancer therapy.

found to exhibit lower gene transfection efficiency due to reduced cellular uptake.[24]

In this study, we report the synthesis and characterization of the histidylated polylysine with reversible-PEGylated cap at one end of polylysine. The basic design is the combination of PEG-detachable polylysine (mPEG-SS-PLL) and histidylated polylysine, as shown in **Scheme 1**. The system is tailored to the key requirements of genetic delivery in vitro and in vivo. The reversible PEGylation allows the protection of the catiomer/pDNA complexes and selective PEG detachment essential to cell internalization.[24,25] The histidylated polylysine exhibits a high buffering capacity favorable for endosome escape, which is a critical step towards cell nucleus. The unique structure of the catiomer enables efficient gene transfection in siRNA–VEGF delivery in vivo.

2. Results and Discussion

2.1. Synthesis of Histidylated Redox-Sensitive Catiomer mPEG-SS-PLH

The redox-sensitive catiomer mPEG-SS-PLL was chosen as the scaffold catiomer with selectively detachable PEGylation. The ultimate gene transfection efficiency by mPEG-SS-PLL is, however, moderate due to limited buffering capacity of PLL. To maximize selective PEG detachment in siRNA–VEGF delivery, the histidine groups, known for high endosome escape ability, were incorporated into the scaffold catiomer mPEG-SS-PLL. This was accomplished by taking advantage of the modifiable primary amines of PLL. The length of the mPEG-SS-PLL blocks was also optimized for high packaging ability.

The synthesis route of the multifaceted catiomer is illustrated in **Figure 1**. Procedurally, mPEG-SS-PzLL52 is prepared by ring-opening polymerization of ε-benzyloxycarbonyl-L-lysine *N*-carboxyanhydride (zLL-NCA) using mPEG-SS-NH_2

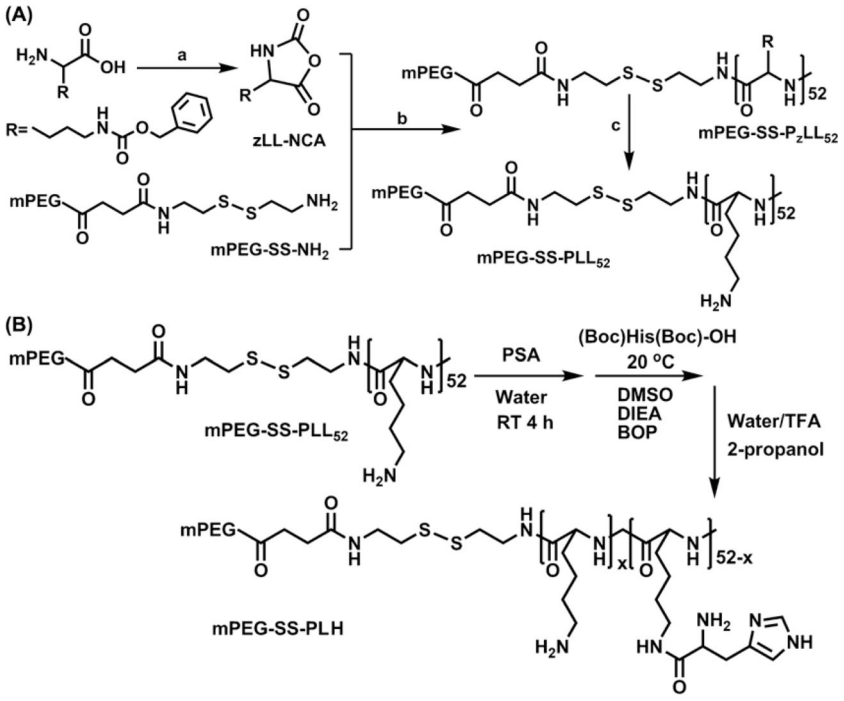

Figure 1. Synthetic scheme of histidylated redox-sensitive catiomer mPEG-SS-PLH, a) zLL/triphosgene = 2.4:1, mol/mol, THF, 50 °C, 4 h; b) zLL-NCA/mPEG-SS-NH_2 = 60:1, mol/mol, DMF, RT, 3 d; c) mPEG-SS-PzLL52, TFA, HBr/HAc, 0 °C, 1 h. B) mPEG-SS-PLL52 is substituted with ε-benzyloxycarbonyl-L-histidine.

Table 1. Molecular weight characteristics of the mPEG-SS-PLH copolymer.

Catiomer	Substitution degree of histidine [%]	$\bar{M}_n$(^{1}H NMR)	$\bar{M}_n$(GPC)	PDI (GPC)
mPEG-SS-PLL52	0	8800	8600	1.064
mPEG-SS-PLH15	29	10 800	10 500	1.144
mPEG-SS-PLH30	58	12 900	12 400	1.099
mPEG-SS-PLH44	85	14 800	14 300	1.013

as initiator. After deprotection, the amino groups in mPEG-SS-PLL52 are first neutralized with 10% *p*-toluence solfonic acid in water, followed by a freeze-drying process to give the *p*-toluenesulfonate salt of mPEG-SS-PLL, which is soluble in DMSO. The histidylation is performed in the presence of ε-benzyloxycarbonyl-L-histidine, DIEA, and BOP in DMSO to afford mPEG-SS-PLH with histidyl residues. Histidyl group is functionally important in mediating vesicular escape, identified as the "proton sponge" mechanism. The number of histidyl residues on one mPEG-SS-PLL52 molecule is optimized by varying the feed ratio of ε-benzyloxycarbonyl-L-histidine to mPEG-SS-PLL52, from 15:1 to 45:1.

Successful synthesis of mPEG-SS-PLL52 and histidylated redox-sensitive catiomer mPEG-SS-PLH with different histidine substitutions is demonstrated by ^{1}H NMR spectrum and gel permeation chromatographic (GPC) analysis, respectively, as shown in Figure S1 (Supporting Information) and **Table 1** (Supporting Information). It is worth noting that this novel vector exhibits negligible cytotoxicity in all tested cells (Figure S2, Supporting Information), a characteristic favorable for in vivo gene therapy.

2.2. Buffering Capacity

Optimal gene transfection requires transfer of the genetic payload into the nucleus. Following cellular internalization, escape from endosomal vesicles represents a major limitation for gene delivery systems. The proton sponge effect has been reported to be a key factor in swelling of the endocytic vesicles, escaping into the cytosol, and therefore affecting the overall gene transfection efficiency.[36,37] Our previous works have shown limited buffering capacity of mPEG-SS-PLL, primarily for lacking of secondary and tertiary amines,[24] which greatly impede the transgene expression. To overcome this critical barrier, reversible-PEGylated histidylated polylysine was developed, with histidyl residues in the structure acting as the proton sponges, in order to enhance the release of payload gene into cytoplasm.

The buffering capacity of mPEG-SS-PLH was evaluated using the conventional acid–base titration method. The results from these titration experiments are summarized in **Figure 2**. Consistent with previous findings,[25] mPEG-SS-PLL52 exhibits a limited buffering capacity attributable to its uniform composition of primary amines. However, after incorporation of histidyl residues, a remarkable increase in buffering capacity of mPEG-SS-PLH catiomer is observed, possibly associated with the intrinsic proton sponge effect of imidazole heterocycle of histidine in the endolysosomal acidic pH range of 4–6.[38–40] In addition, the buffering capacity of mPEG-SS-PLH catiomers has a slight increase with increasing histidine substitution. These results indicate that histidylation can efficiently increase the buffering capacity of mPEG-SS-PLL, facilitating genetic payload release into cytoplasm.

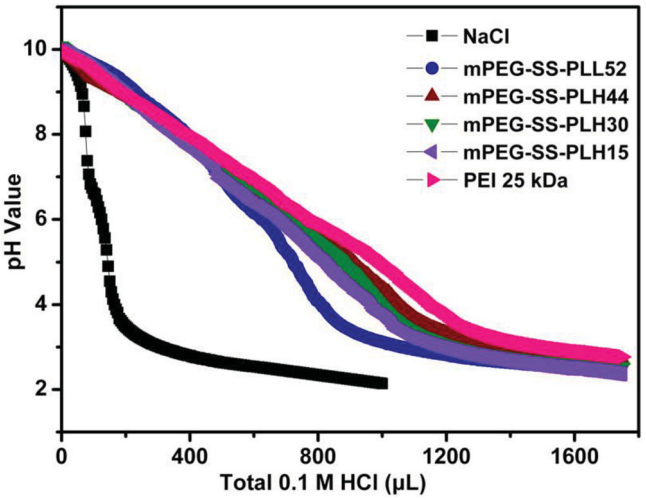

Figure 2. Buffering capacity of catiomers. Polymer solutions (200 mg L^{-1}) are adjusted to pH 10 using 0.1 M NaOH. Subsequently, aliquots of 0.1 M HCl are added, and solution pH is recorded. Representative plots are shown for different histidylated redox-sensitive catiomer mPEG-SS-PLH and bPEI-25k.

2.3. DNA Binding Ability of mPEG-SS-PLH

Electrostatic interactions between negatively charged DNA and positively charged polymers facilitate the formation of partially or completely neutralized association polyplexes. As a consequence, successful condensation of DNA with catiomers results in retardation or complete loss of oriented migration of DNA within an electric field. The results in **Figure 3** show that DNA migration is efficiently inhibited by the mPEG-SS-PLL52/pDNA complexes at a weight ratio >0.5 (Panel A), indicating effective DNA condensation. This finding is consistent with the previous report that polycations with a high p*Ka* value (>9.0), such as PLL, form stable polyplexes even at the lower N/P ratio. In contrast, polycations with lower p*Ka* values generally have a weak affinity to DNA, and polyplexes is easily dissociated under the physiological conditions.[41] Histidine with a p*Ka* (≈6.0) is not electrically charged at pH 7.4,[42] leading to reduced DNA condensation ability of histidylated polycations. As expected, mPEG-SS-PLH exhibits a weaker DNA condensation ability compared to mPEG-SS-PLL52. mPEG-SS-PLH15 (the number in the compound notation represents substitution of histidine) reaches complete condensation of pDNA at the weight ratio >1 (Panel D). Furthermore, a notable decrease in DNA binding ability was observed at higher histidine substitution (Panels B,C). For example, mPEG-SS-PLH30 reaches complete retardation of pDNA at a weight ratio ≥2, while that of PEG-SS-PLH44 ≥4. Therefore, histidylation is accordingly optimized by structural design, synthesis, and processing for buffering capacity and DNA condensation.

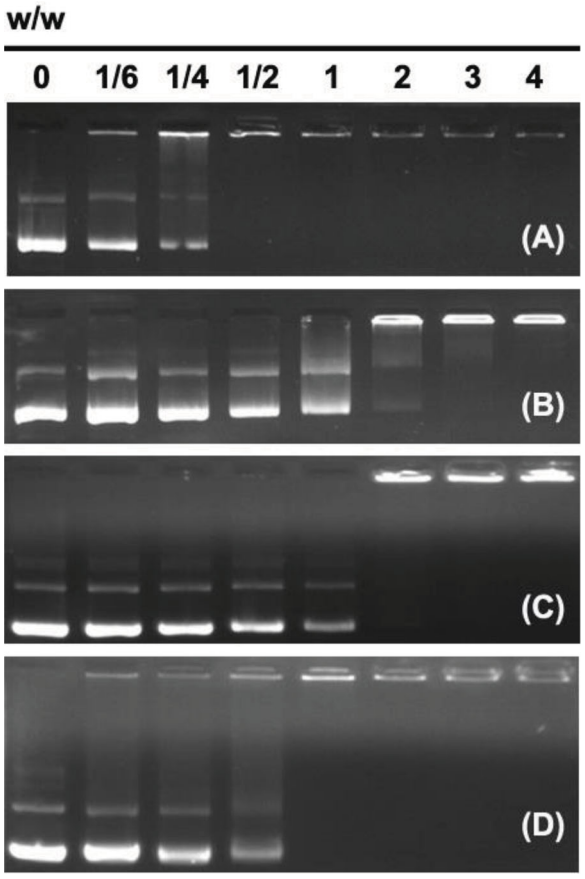

Figure 3. DNA complexation with histidylated redox-sensitive catiomer mPEG-SS-PLH. Agarose gel retardation is performed as outlined in the Experimental Section using mixtures of A) mPEG-SS-PLL52; B) mPEG-SS-PLH44; C) mPEG-SS-PLH30; and D) mPEG-SS-PLH15 with pDNA prepared at weight ratios ranging from 0:1 to 4:1. Representative gels are visualized at $\lambda = 254$ nm.

2.4. Complexes of pDNA with mPEG-SS-PLH Catiomers

The particle size and surface charge of catiomer/pDNA polyplexes are known to strongly influence cytotoxicity, cellular uptake, intracellular trafficking, release of genetic payload, and subsequent transfection efficiency.[43] The morphometric analysis of mPEG-SS-PLH/pDNA complexes was performed by transmission electron microscopy (TEM) and dynamic light scattering (DLS).

Figure S3A (Supporting Information) insert shows TEM images of the spherical aggregates with diameters of 60 ± 10 nm. The dynamic hydration diameter of 180 nm is determined by DLS (Figure S3A, Supporting Information), which is believed to be within the optimum size range associated with efficient cellular uptake.[44] The apparent discrepancy in size characteristics between the two methods, namely TEM and DLS, is due to evaporation of water required for TEM sample preparation. In addition, the particle sizes of all catiomer/pDNA complexes have a similar tendency with the increasing weight ratios. As shown in Figure S3B (Supporting Information), the particle size decreases with increasing weight ratios, and the average particle size is less than 220 nm at the weight ratio ≥2:1. In parallel, the zeta potential of these complexes significantly increases from −30 to +20 mV when catiomer/pDNA weight ratio is increased from 0.15:1 to 4:1 (Figure S3C, Supporting Information). The dramatic shift in zeta potential indicates gradual neutralization of negative charge of polymer-associated pDNA. The neutralization appears at a weight ratio of 2:1. These results are consistent with previous eletrophoretic mobility data shown in Figure 3D. Further increase in catiomer content leads to an excess of positively charged amine groups on the surfaces of the polyplexes. Eventually, charge–charge repulsion limits particle formation to a mean diameter less than 220 nm and zeta potential of +20 mV. It should be noted that throughout the entire weight ratio range tested, the mPEG-SS-PLH/pDNA polyplexes always maintain a lower zeta potential compared to that of mPEG-SS-PLL52/pDNA, primarily owing to the neutral histidyl residues at pH 7.4. In general, the optimum particle size and zeta potential of catiomer/pDNA complexes can facilitate the effective internalization into the desired targeted cells.

2.5. Transfection Efficiency of mPEG-SS-PLH Polyplexes

In vitro transfection experiments were performed on 293T, MCF-7, and PC-3 cells using EGFP as reported gene, and bPEI-25k at its optimal weight ratio 1.3:1 as the control. The catiomer/pEGFP weight ratio in the range of 1:1 to 5:1 was used for flow cytometry assay, which is higher than that at complete DNA retardation. The weight ratios ranging from 1:1 to 7:1 were used for fluorescence intensity analysis.

The high densities of fluorescent cells visible under the microscope after transfection in mPEG-SS-PLL52-, mPEG-SS-PLH-, and PEI-based polyplexes demonstrate successful delivery of pEGFP into the nucleus of 293T, MCF-7, and PC-3 cells (Figure S4, Supporting Information). However, the transfection efficiency of these polyplexes varies among different cell types. A higher transfection activity is observed in the 293T cell line. Figure S4 (Supporting Information) also shows the key role of histidine substitution in gene transfer ability of mPEG-SS-PLL52 and mPEG-SS-PLL15. The latter was substituted with 15 histidyl residues, identified as mPEG-SS-PLH15. It exhibits remarkable enhancement in transfection efficiency. However, mPEG-SS-PLL52 substituted with 44 histidyl residues, identified as mPEG-SS-PLH44, experiences a significant reduction in transfection efficiency. The possible reason is ascribed to the increased histidine substitution for reduced DNA binding ability and stability.

A similar tendency of EGFP-expression profiles is observed in the flow cytometry results (**Figure 4**), where gene transfection efficiency exhibits a cell-type dependence and a higher transfection activity is observed in the 293T cell line. For example, the calculated transfection efficiencies of viable cells in MCF-7 and PC-3 cells are between 22%–28% and 8%–17%, respectively, for the mPEG-SS-PLL52-based polyplexes. In contrast, those of viable cells in 293T are in the range of 40%–55% for the same polyplexes. Furthermore, the gene expression increases with increasing catiomer/pDNA weight ratio and gradually approaches saturation. It should be noted that the excess

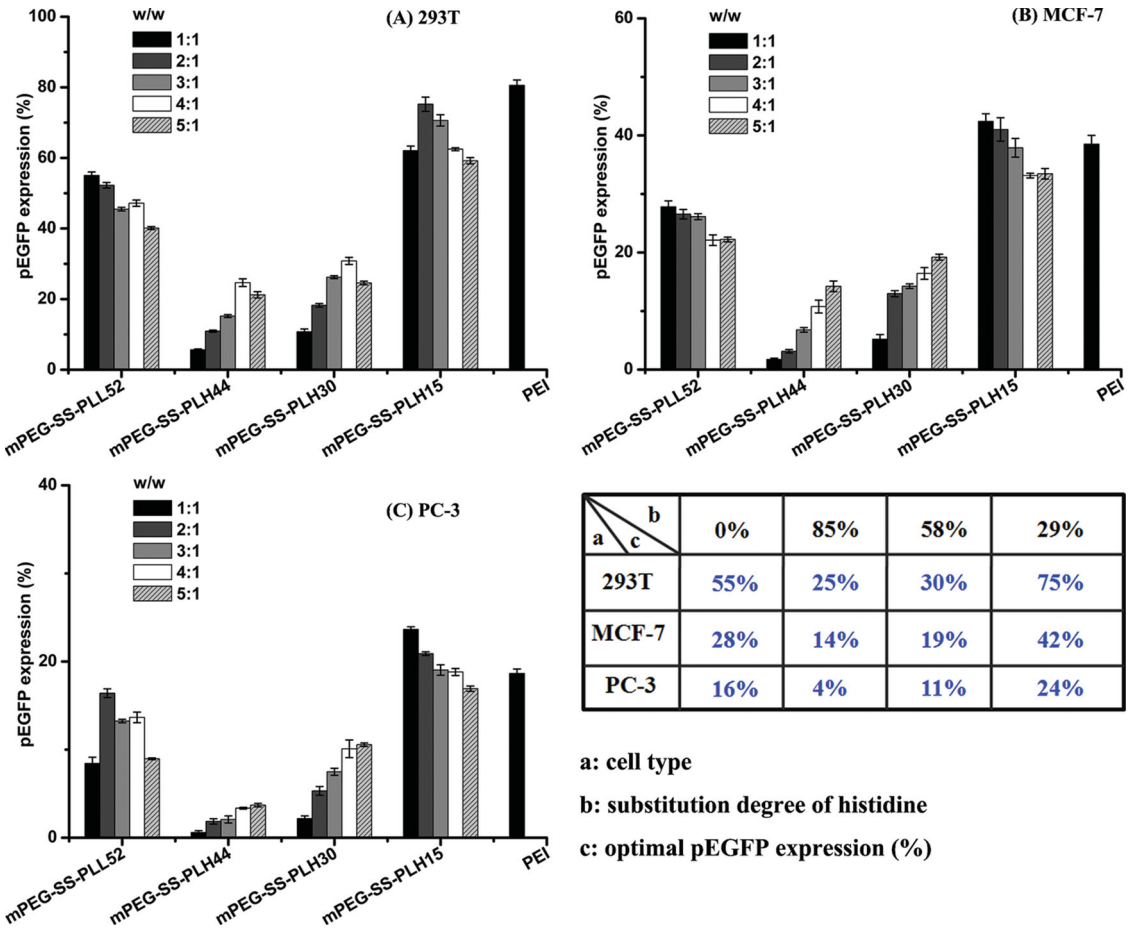

a \ b / c	0%	85%	58%	29%
293T	55%	25%	30%	75%
MCF-7	28%	14%	19%	42%
PC-3	16%	4%	11%	24%

a: cell type

b: substitution degree of histidine

c: optimal pEGFP expression (%)

Figure 4. Transfection efficiency of histidylated redox-sensitive catiomer mPEG-SS-PLH-based/pDNA polyplexes. 293T, MCF-7, and PC-3 cells are incubated for 4 h with mPEG-SS-PLL52/pEGFP, mPEG-PLH44/pEGFP, mPEG-SS-PLH30/pEGFP, and mPEG-SS-PLH15/pEGFP complexes at weight ratios ranging from 1:1 to 5:1. PEI/pEGFP is used as control. Viable pEGFP-expressing cells are quantified after transfection for 44 h using flow cytometry and normalized to viable control cells (B). Data are shown as mean ± SD ($n = 3$).

cationic polymer limits pDNA release from the polyplexes, due to increased stability of the associated polyplexes.[45] A higher zeta potential can also decrease the gene transfer ability due to cytotoxicity or activation of some unknown deleterious cellular response.

The flow cytometry experimental results indicate an important relationship between histidine substitution and the gene transfection profiles. The transfection activities of mPEG-SS-PLL52 in 293T cells are 1.8- and 2.2-fold lower when substituted, respectively, with 30 histidyl and 44 histidyl residues. In contrast, that of mPEG-SS-PLL52 in 293T cells is about 1.4-fold higher when substituted with 15 histidyl residues. The highest transfection efficiencies of mPEG-SS-PLH15 in 293T, MCF-7, and PC-3 cells are 75%, 42%, and 24%, respectively. These are even higher than those of bPEI-25k (38.5% and 20%) in MCF-7 and PC-3 cells. The redox-sensitive catiomer mPEG-SS-PLL, with optimal histidine substitution, is therefore capable of extremely high transfection efficacies in vitro.

EGFP expression was further quantified spectrofluorometrically at an excitation wavelength of 488 nm and emission of 509 nm. As shown in Figure S5 (Supporting Information), there is a similar trend that gene transfection experiences cell type and weight ratio dependencies. The gene transfection profiles of mPEG-SS-PLL52 are found to be improved ≈1.3-fold in all three cell lines when substituted with 15 histidyl residues. Those are of ≈1.4- and ≈1.5-fold lower when substituted with 30 histidyl and 44 histidyl residues, respectively. Importantly, mPEG-SS-PLH15 also exhibits the maximum gene expression in all three cell lines, greater than that of bPEI-25k.

To achieve high stability of gene vectors in serum is a major goal in the design of the reversible PEGylation, which is essential to in vivo circulation.[46,47] In this study, the effects of serum on the stability of the mPEG-SS-PLH/pDNA polyplexes were assessed in the absence and presence of 10% serum. As shown in **Figure 5**, the transfection activities of mPEG-SS-PLL52, mPEG-SS-PLH44, mPEG-SS-PLH30, and mPEG-SS-PLH15 are slightly affected by serum. This is possibly due to the PEG-shielding effect and incorporation of histidyl residues. However, the transfection efficiencies of bPEI-25k are ≈2.8-, ≈2.4-, and ≈2.3-fold lower in the presence of 10% serum for 293T, MCF-7, and PC-3 cell lines, respectively. Reduction in transfection efficiency of bPEI-25k/pDNA polyplexes is likely attributed to its instability in serum for their high surface charges.[48]

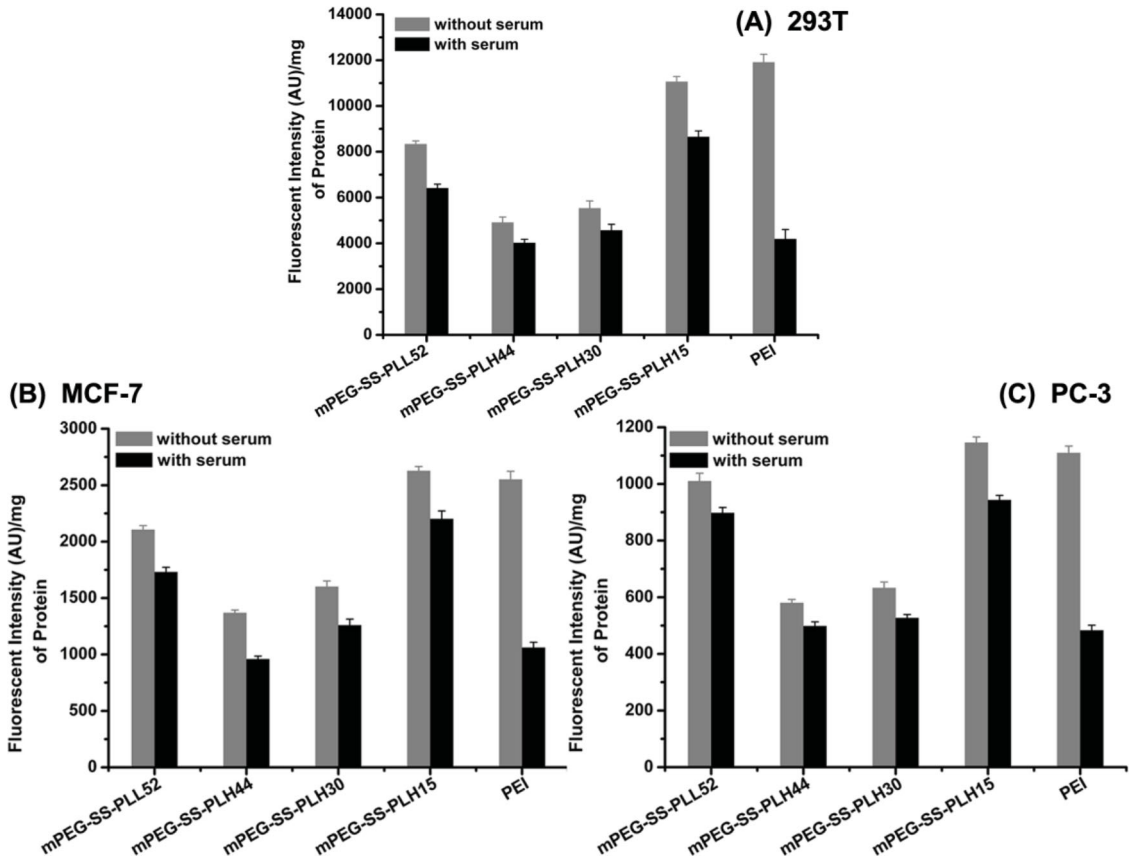

Figure 5. Effects of serum on transfection efficiency of histidylated redox-sensitive catiomer mPEG-SS-PLH-based/pDNA polyplexes. 293T, MCF-7, and PC-3 cells are incubated for 4 h with mPEG-SS-PLL52/pEGFP, mPEG-PLH44/pEGFP, mPEG-SS-PLH30/pEGFP, and mPEG-SS-PLH15/pEGFP complexes, each at its optimal weight ratio. PEI/pEGFP is used as control. Fluorescent intensity of GFP fluorophore in the cell lysate is measured using spectrofluorometer, and the results are expressed in terms of arb unit/mg total cellular protein. Data are shown as mean ± SD ($n = 3$).

2.6. Observation of Intracellular DNA Transport

To visualize intracellular DNA transport, aided by the histidylated redox-sensitive catiomer mPEG-SS-PLH, Cy3-labeled EGFP was prepared following a protocol published previously.[43] The fluorescently labeled EGFP is traceable under biological conditions. Before observation by confocal laser scanning microscopy, MCF-7 cells were first incubated for 4 h with mPEG-SS-PLH and the PEI-based complexes fabricated at each optimal catiomer/pDNA weight ratio. The cells were counterstained with DAPI for cell nuclei and Lysotracker Green for acidic organelles. Confocal images show that Cy3-labeled pDNA signal (**Figure 6**, panel 1) can be detected in all cells after 4 h of treatment. In particular, co-localization of polyplexes in endosome is observed in yellow from the overlap of green and red images (Figure 6, Panel 4). As shown in Figure 6, Panel A4, most of the nuclear fluorescent signal is mainly localized in the perinuclear area, in contrast to the DPAI signal in the nucleus. The Cy3-labeled pDNA signal is observed from the nucleus of MCF-7 cells for mPEG-SS-PLH44/pDNA and mPEG-SS-PLH15/pDNA complexes (Figure 6, Panels B4,C4). These results indicate efficient endosome escape of mPEG-SS-PLH-based polyplexes due to histidyl residues, which is responsible for the increased nuclear transport efficiency.

2.7. Biological Efficiency of mPEG-SS-PLH Polyplexes in HeLa Cells

In vivo gene transfection and in vivo antitumor effect experiments were conducted in tumor-bearing mice. In order to determine the optimal weight ratio for in vivo experiments, the fluorescence intensity analysis was performed in HeLa cells using pEGFP as the reporter gene in absence or presence of 10% FBS. As shown in Figure S6A (Supporting Information), the high density of fluorescent cells visible under the microscope, after transfection with mPEG-SS-PLH15/pEGFP polyplexes, indicates successful delivery of pEGFP into the nucleus of HeLa cells. More importantly, the presence of serum has a negligible effect on the biological efficiency of mPEG-SS-PLH vector. At its optimal weight ratio of 2:1, there is only 13% reduction in fluorescent intensity, as shown in Figure S6B, which is acceptable for in vivo gene delivery.

siRNA technology[49] has been a powerful tool in treatment of various gene-related diseases including infectious and cancers.[29,50,51] Moreover, siRNA targeting VEGF can specifically suppress VEGF expression in many different types of cancer cells.[52–55] However, an effective delivery system is essential to a significant RNAi effect. In vitro transfection has shown that mPEG-SS-PLH15 is capable of efficient delivery of pEGFP into

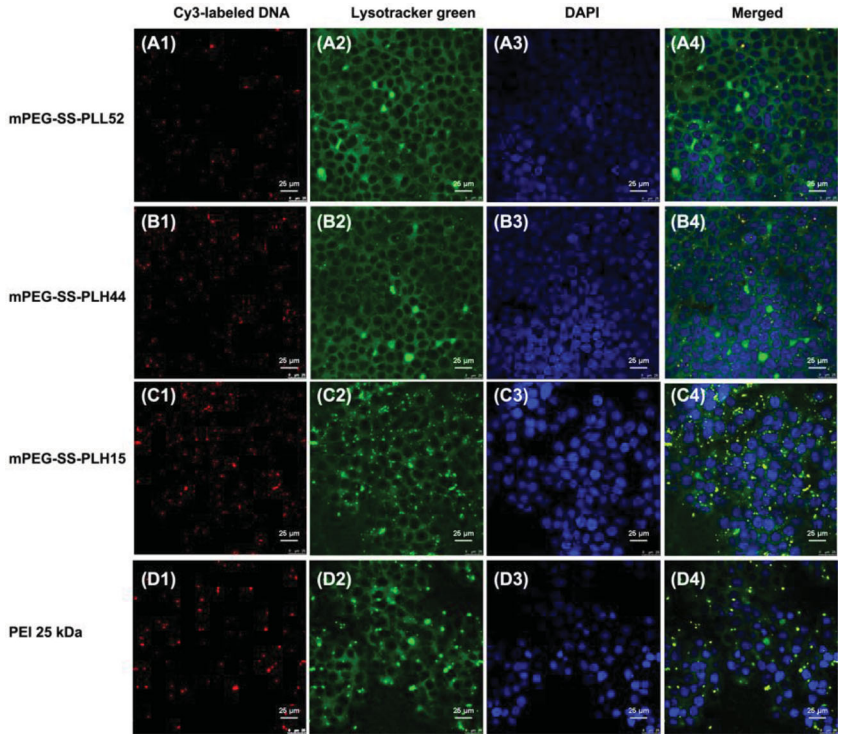

Figure 6. Confocal microscopy images of intracellular trafficking of histidylated redox-sensitive catiomer mPEG-SS-PLH-based polyplexes. MCF-7 cells are incubated for 4 h with mPEG-SS-PLL52/pEGFP (Panel A), mPEG-SS-PLH44/pEGFP (Panel B), and mPEG-SS-PLH15/pEGFP (Panel C) polyplexes fabricated at each optimum weight ratio. PEI/pEGFP (1.3:1, w/w) is used as control (D).

the nucleus of 293T, MCF-7, and PC-3 cells. This type of vector was utilized in this study to deliver siRNA–VEGF for in vitro and in vivo cancer therapy.

The VEGF expression inhibition activity of mPEG-SS-PLH15/siRNA–VEGF complexes was characterized by using western blot assay. As shown in **Figure** 7I, VEGF expression is distinctly suppressed in the mPEG-SS-PLH15 group. For the mPEG-SS-PLL52 group, the inhibition effect is also detected, but not as pronounced as in the mPEG-SS-PLH15 group. These results are consistent with the transfection experiments.

The in vitro therapy, mediated by mPEG-SS-PLH15/siRNA–VEGF and mPEG-SS-PLL52/siRNA–VEGF, was investigated in HeLa cells by MTT assay. mPEG-SS-PLH15 and mPEG-SS-PLL52, with a concentration in the range from 4 to 60 μg mL^{-1}, were used for comparison. As shown in Figure 7II, no significant decrease of cell viability is observed in cells treated with pure mPEG-SS-PLH15 and mPEG-SS-PLL52. The cell viability is found to be more than 90% even at the highest vector concentration of 60 μg mL^{-1}. However, for cells treated with mPEG-SS-PLL52/siRNA–VEGF and mPEG-SS-PLH15/siRNA–VEGF, the cell viability decreases gradually with the increasing concentration of siRNA–VEGF. Only 26% cell viability is detected for cells treated with mPEG-SS-PLH15/siRNA–VEGF at the highest siRNA–VEGF concentration of 30 μg mL^{-1}. These results suggest the key role of siRNA–VEGF in the treatment of HeLa cells, and its significant inhibition effects on the proliferation of HeLa cells.

2.8. Biodistribution of mPEG-SS-PLH15 in Tumor-Bearing Mice

Biodistribution of mPEG-SS-PLH15 in tumor-bearing mice is shown in **Figure 8**. The time dependence shows rapid transport of catiomer in the tumor-bearing mice after intravenous injection without obvious aggregation in the localized regions. Shortly after injection, the catiomer is found in main tissues including the tumor. These observations indicate the biological stability of the catiomer. Liver, spleen, and kidney are also the primary organs in which strong fluorescence signals are detected in vivo after tail-vein injection of BODIPY-labeled mPEG-SS-PLH15.

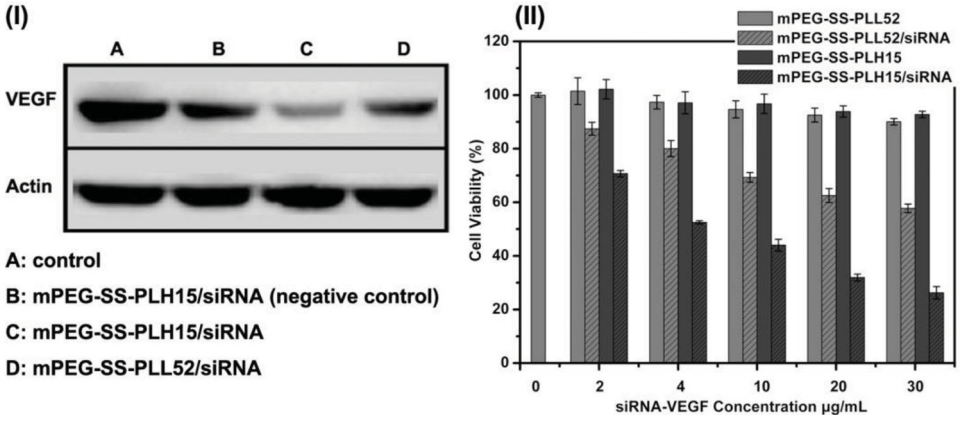

Figure 7. Western blot analysis (I) in HeLa cells by control (A), mPEG-SS-PLH15/scrambled siRNA (negative control) (B), mPEG-SS-PLH15/siRNA–VEGF (C), and mPEG-SS-PLL52/siRNA–VEGF (D). Cell viabilities after transfected by mPEG-SS-PLL52, mPEG-SS-PLL52/siRNA–VEGF, mPEG-SS-PLH15, and mPEG-SS-PLH15/siRNA–VEGF in HeLa cells for 48 h (II). Data are shown as mean ± SD ($n = 5$).

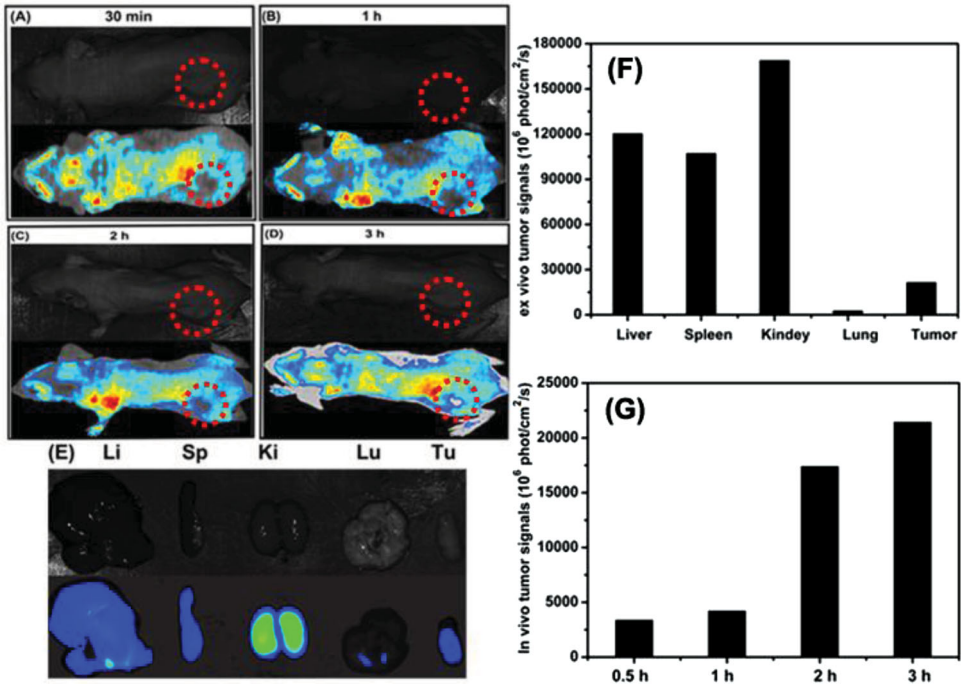

Figure 8. In vivo distribution in mice with subcutaneous xenograft at A) 30 min, B) 1 h, C) 2 h, and D) 3 h after intravenous injection of 200 μg BODIPY-labeled mPEG-SS-PLH15. The image of isolated organs at 3 h with E) BODIPY-labeled mPEG-SS-PLH15. Li, Sp, Ki, Lu, and Tu indicate liver, spleen, kidney, lung, and tumor, respectively. The fluorescence signal intensity is measured for excised organs (F) and in vivo tumor (G). The excitation and emission wavelengths of BODIPY dye are 650/665 nm, respectively.

2.9. In Vivo Gene Expression in Tumor-Bearing Mice

Seven days after intravenous administration of polyplexes, GFP expression in sections of important organs and xenograft is observed as shown in **Figure 9**. GFP expression is found in liver, spleen, kidney, lung, and tumor of the mice, treated with the mPEG-SS-PLH15 vector. The fluorescence intensities in liver, spleen, and kidney are found to be much stronger than those in other organs. This behavior is possibly associated with the reticuloendothelial system (RES) or mononuclear phagocyte system (MPS). Relatively high fluorescence intensity is also observed in tumor.

2.10. In Vivo Antitumor Effect

The therapeutic efficacy of mPEG-SS-PLH15/siRNA-VEGF and mPEG-SS-PLL52/siRNA-VEGF was further evaluated by monitoring tumor growth in an animal model via intravenous and intratumoral injection. A dose of 20 μg of siRNA-VEGF was intravenously and intratumorally administered in mice every 2 d. The two control groups were, respectively, injected with 150 μL of PBS or mPEG-SS-PLH15 containing 20 μg scrambled control siRNA. The tumor volume is measured at regular intervals.

The tumor suppression effect is found to be highly dependent on the vector/DNA formulations.[56] As shown in **Figure 10**I, upon intravenous administration, at the maximum experimental period, different xenograft tumor sizes are found as follows: 287 mm^3 in the PBS group, 178 mm^3 in the mPEG-SS-PLL52/siRNA–VEGF group, and 102 mm^3 in the

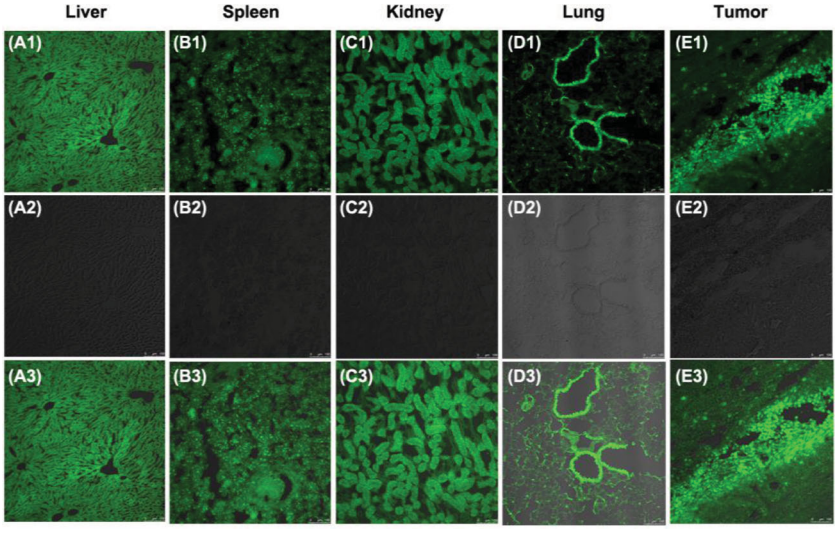

Figure 9. Confocal microscopy images of transfected sections of A) liver, B) spleen, C) kidney, D) lung, and E) tumor after intravenous injection of mPEG-SS-PLH15/pEGFP complexes (green, 2:1, dose: 100 μg pEGFP per mice) 7 d. Row 1 and Row 2 show the images of the fluorescent and bright field, respectively. Images of Row 3 are merged images of Row 1 and Row 2. Images are captured at 20×.

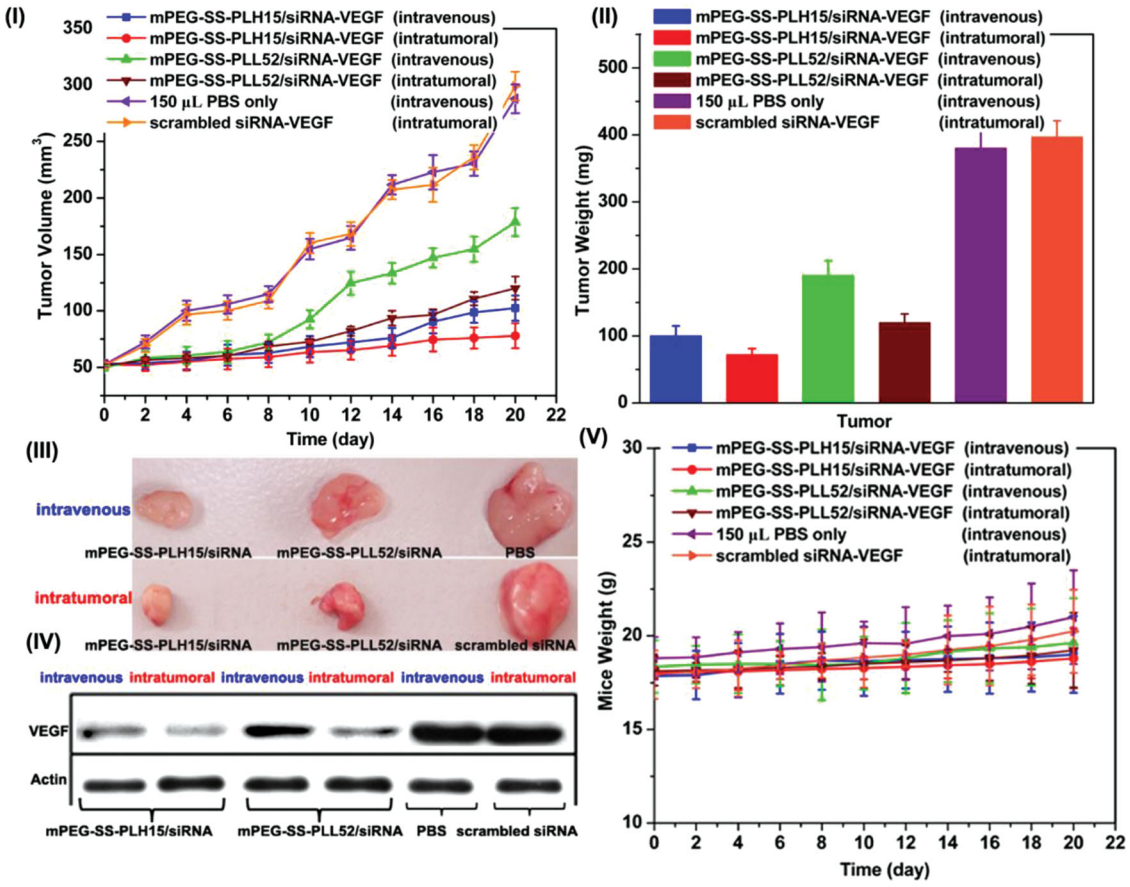

Figure 10. I) Tumor volume and II) tumor weight of HeLa xenograft nude mice after intravenous and intratumoral treatment with different vector/siRNA–VEGF complexes. III) Photograph and IV) VEGF expression of tumors in HeLa xenograft nude mice after intravenous and intratumoral treatment with different vector/siRNA–VEGF complexes. V) Mice weight of HeLa xenograft nude mice after intravenous and intratumoral treatment with different vector/siRNA–VEGF complexes. PBS and mPEG-SS-PLH15 loaded with scrambled sequence are served as negative controls.

mPEG-SS-PLH15/siRNA–VEGF group. The tumor growth is effectively suppressed as shown in this figure. High therapeutic efficacy is also observed via intratumoral administration. For example, at the maximum experimental period, the xenograft tumor sizes are: 120 mm^3 in the mPEG-SS-PLL52/siRNA–VEGF group, 78 mm^3 in the mPEG-SS-PLH15/siRNA–VEGF group, and 299 mm^3 in the scrambled siRNA group.

Figure 10II shows the inhibitory effect exerted by siRNA–VEGF infection in terms of tumor weight. Compared with the control group, tumor weight is significantly lower. On the last day of experiment, the tumor weights for the groups intravenously injected with mPEG-SS-PLL52/siRNA–VEGF and mPEG-SS-PLH15/siRNA–VEGF have been, respectively, reduced to 50% and 26%. Intratumoral administration has resulted in tumor reduction of 30% and 18%, respectively, for the groups injected with mPEG-SS-PLL52/siRNA–VEGF and mPEG-SS-PLH15/siRNA–VEGF.

HeLa tumors were photographed ex vivo. A representative tumor from each group is shown in Figure 10III. The mPEG-SS-PLH15 group shows dramatic inhibiting effect via both intravenous and intratumoral injections, as expected from neovascularization. mPEG-SS-PLH15/siRNA–VEGF exhibits the most pronounced effect on microvessel suppression compared to the PBS and scrambled siRNA group. The mPEG-SS-PLL52 group also exhibits sufficient microvessel suppression via intratumoral injection. These results are consistent with the in vivo VEGF expression levels as shown in Figure 10IV. As can be seen in this figure, VEGF expression is well suppressed by the mPEG-SS-PLH15 group via both intravenous and intratumoral injection. VEGF expression is also detected in the mPEG-SS-PLL52 group, but intratumoral injection results in stronger inhibition effect compared to the intravenous injection route.

No significant difference in body weight is observed between the mice treated with mPEG-SS-PLL52, mPEG-SS-PLH15, and the control group for the experimental period indicated, as shown in Figure 10V.

3. Conclusions

In this study, a gene delivery vector, namely the reversible-PEGylated histidylated polylysine, has been designed according to the specific gene delivery requirements and successfully developed for cancer therapy. The reversible-PEGylation allows the protection of the catiomer/pDNA complexes and selective PEG detachment, which is essential to cell internalization. Histidylation has significantly enhanced the biological efficacy of mPEG-SS-PLL catiomer due to effective endosomal escape.

The experimental results show effective inhibition of cancer cell proliferation in vitro and tumor growth in vivo by mPEG-SS-PLH. The delivery system developed in this study shows promise for clinical applications.

Supporting Information

Supporting Information is available from the Wiley Online Library or from the author.

Acknowledgements

X.J.C. and H.Y.Z. contributed equally to this work. This work was financially supported by the 973 program (2013CB967500), the National Natural Science Foundation of China (21104059 and 51173136), Shanghai Rising-Star Program (12QA1403400) and "Chen Guang" project founded by Shanghai Municipal Education Commission and Shanghai Education Development Foundation.

Received: January 30, 2014
Published online: May 7, 2014

[1] J. Yang, H. Y. Wang, W. J. Yi, Y. H. Gong, X. Zhou, R. X. Zhuo, X. Z. Zhang, *Adv. Healthcare Mater.* **2013**, *2*, 481.
[2] P. Saccardo, A. Villaverde, N. Gonzalez-Montalban, *Biotechnol. Adv.* **2009**, *27*, 432.
[3] S. Y. Tzeng, J. J. Green, *Adv. Healthcare Mater.* **2013**, *2*, 468.
[4] F. Y. Dai, W. G. Liu, *Biomaterials* **2011**, *32*, 628.
[5] H. Y. Tian, Z. P. Guo, J. Chen, L. Lin, J. L. Xia, X. Dong, X. S. Chen, *Adv. Healthcare Mater.* **2012**, *1*, 337.
[6] C. Yang, W. Cheng, P. Y. Teo, A. C. Engler, D. J. Coady, J. L. Hedrick, Y. Y. Yang, *Adv. Healthcare Mater.* **2013**, *2*, 1304.
[7] J. L. Xia, H. Y. Tian, L. Chen, L. Lin, Z. P. Guo, J. Chen, X. S. Chen, *Biomacromolecules* **2011**, *12*, 1024.
[8] C. L. Fu, L. Lin, H. L. Shi, D. X. Zheng, W. Wang, S. Q. Gao, Y. F. Zhao, H. Y. Tian, X. J. Zhu, X. S. Chen, *Biomaterials* **2012**, *33*, 4589.
[9] H. Y. Tian, J. Chen, X. S. Chen, *Small* **2013**, *9*, 2034.
[10] C. Dufes, I. F. Uchegbu, A. G. Schatzlein, *Adv. Drug Delivery Rev.* **2005**, *57*, 2177.
[11] G. Navarro, C. Tros de ILarduya, *Nanomedicine* **2009**, *5*, 287.
[12] K. Luo, C. X. Li, G. Wang, Y. Nie, B. He, Y. Wu, Z. W. Gu, *J. Controlled Release* **2011**, *155*, 77.
[13] M. Sanjoh, S. Hiki, Y. Lee, M. Oba, K. Miyata, T. Ishii, K. Kataoka, *Macromol. Rapid Commun.* **2010**, *31*, 1181.
[14] X. Zhang, M. Oulad-Abdelghani, A. N. Zelkin, Y. J. Wang, Y. Haikel, D. Mainard, J. C. Voegel, F. Caruso, N. Benkirane-Jessel, *Biomaterials* **2010**, *31*, 1699.
[15] M. L. Patil, M. Zhang, T. Minko, *ACS Nano* **2011**, *5*, 1877.
[16] C. M. Wiethoff, C. R. Middaugh, *J. Pharm. Sci.* **2003**, *92*, 203.
[17] M. E. Martin, K. G. Rice, *AAPS J.* **2007**, *9*, E18.
[18] M. A. Mintzer, E. E. Simanek, *Chem. Rev.* **2009**, *109*, 259.
[19] D. Luo, W. M. Saltzman, *Nat. Biotechnol.* **2000**, *18*, 33.
[20] A. Barnard, P. Posocco, S. Pricl, M. Calderon, R. Haag, M. E. Hwang, V. W. T. Shum, D. W. Pack, D. K. Smith, *J. Am. Chem. Soc.* **2011**, *133*, 20288.
[21] C. M. Ward, M. L. Read, L. W. Seymour, *Blood* **2001**, *97*, 2221.
[22] T. Merdan, J. Kopecek, T. Kissel, *Adv. Drug Delivery Rev.* **2002**, *54*, 715.
[23] D. Z. Zhou, C. X. Li, Y. L. Hu, H. Zhou, J. T. Chen, Z. P. Zhang, T. Y. Guo, *J. Mater. Chem.* **2012**, *22*, 10743.
[24] X. J. Cai, H. Q. Dong, W. J. Xia, H. Y. Wen, X. Q. Li, J. H. Yu, Y. Y. Li, D. L. Shi, *J. Mater. Chem.* **2011**, *21*, 14639.
[25] X. J. Cai, C. Y. Dong, H. Q. Dong, G. M. Wang, G. M. Pauletti, X. J. Pan, H. Y. Wen, I. Mehl, Y. Y. Li, D. L. Shi, *Biomacromolecules* **2012**, *13*, 1024.
[26] X. J. Cai, H. Q. Dong, J. P. Ma, H. Y. Zhu, W. Wu, M. Chu, Y. Y. Li, D. L. Shi, *J. Mater. Chem. B.* **2013**, *1*, 1712.
[27] L. J. Scherer, J. J. Rossi, *Nat. Biotechnol.* **2003**, *21*, 1457.
[28] N. Ferrara, H. P. Gerber, J. Lecouter, *Nat. Med.* **2003**, *9*, 669.
[29] H. Y. Wang, W. J. Yi, S. Y. Qin, C. Li, R. X. Zhuo, X. Z. Zhang, *Biomaterials* **2012**, *33*, 8685.
[30] P. Midoux, M. Monsigny, *Bioconjugate Chem.* **1999**, *10*, 406.
[31] I. Fajac, J. C. Allo, M. Merten, C. Pichon, C. Figarella, M. Monsigny, P. Briand, P. Midoux, *J. Gene Med.* **2000**, *2*, 368.
[32] M. B. Roufai, P. Midoux, *Bioconjugate Chem.* **2001**, *12*, 92.
[33] J. M. Benns, J. S. Choi, R. I. Mahato, J. S. Park, S. W. Kim, *Bioconjugate Chem.* **2000**, *11*, 637.
[34] M. Bikram, C. H. Ahn, S. Y. Chae, M. Lee, J. W. Yockman, S. W. Kim, *Macromolecules* **2004**, *37*, 1903.
[35] J. Dai, S. Y. Zou, Y. Y. Pei, D. Cheng, H. Ai, X. T. Shuai, *Biomaterials* **2011**, *32*, 1694.
[36] D. W. Pack, D. Putnam, R. Langer, *Biotechnol. Bioeng.* **2000**, *67*, 217.
[37] C. Moreira, H. Oliveira, L. R. Pires, S. Simoes, M. A. Barbosa, A. P. Pego, *Acta Biomater.* **2009**, *5*, 267.
[38] Y. X. Yang, Z. W. Zhang, L. L. Chen, Y. P. Li, *Int. J. Pharm.* **2010**, *390*, 191.
[39] S. Asayama, T. Kumagai, H. Kawakami, *Bioconjugate Chem.* **2012**, *23*, 1437.
[40] J. J. Gu, X. Wang, X. J. Jiang, Y. Z. Chen, L. C. Chen, X. L. Fang, X. Y. Sha, *Biomaterials* **2012**, *33*, 644.
[41] K. Osada, K. Kataoka, *Adv. Polym. Sci.* **2006**, *202*, 113.
[42] S. Asayama, T. Kumagai, H. Kawakami, S. Nagaoka, *Bioconjugate Chem.* **2007**, *18*, 1662.
[43] R. L. Sheng, T. Luo, Y. D. Zhu, H. Li, J. J. Sun, S. D. Chen, W. Y. Sun, A. Cao, *Biomaterials* **2011**, *32*, 3507.
[44] Y. M. Liu, T. M. Reineke, *J. Am. Chem. Soc.* **2005**, *127*, 3004.
[45] B. Lu, X. D. Xu, X. Z. Zhang, S. X. Cheng, R. X. Zhuo, *Biomacromolecules* **2008**, *9*, 2594.
[46] K. Miyata, M. Oba, M. R. Kano, S. Fukushima, Y. Vachutinsky, M. Han, H. Koyama, K. Miyazono, N. Nishiyama, K. Kataoka, *Pharm. Res.* **2008**, *25*, 2924.
[47] S. Fukushima, K. Miyata, N. Nishiyama, N. Kanayama, Y. Yamasaki, K. Kataoka, *J. Am. Chem. Soc.* **2005**, *127*, 2810.
[48] D. Fischer, T. Bieber, Y. Li, H. P. Elsasser, T. Kissel, *Pharm. Res.* **1999**, *16*, 1273.
[49] S. M. Elbashir, J. Harborth, K. Weber, T. Tuschl, *Methods* **2002**, *26*, 199.
[50] B. Dalby, S. Cates, A. Harris, E. C. Ohki, M. L. Tilkins, P. J. Price, V. C. Ciccarone, *Methods* **2004**, *33*, 95.
[51] M. Izquierdo, *Cancer Gene Ther.* **2005**, *12*, 217.
[52] P. Sun, J. Gao, Y. L. Liu, L. W. Wei, L. P. Wu, Z. Y. Liu, *Mol. Cell Biochem.* **2008**, *308*, 161.
[53] S. H. Kim, S. H. Lee, H. Tian, X. Chen, T. G. Park, *J. Drug Target* **2009**, *17*, 311.
[54] M. R. Hasan, S. H. Ho, D. A. Owen, I. T. Tai, *Int. J. Cancer* **2011**, *129*, 2115.
[55] E. Raskopf, A. Vogt, T. Sauernruch, V. Schmitz, *J. Hepatol.* **2008**, *49*, 977.
[56] Y. H. Huang, G. T. Zugates, W. Peng, D. Holta, C. Dunton, J. J. Green, N. Hossain, M. R. Chernick, R. F. Padera Jr., R. Langer, D. G. Anderson, J. A. Sawicki, *Cancer Res.* **2009**, *69*, 6184.

